**Analyst**

# DNA Hybridization Detection with 100 zM Sensitivity Using Piezoelec-
# tric Plate Sensors with Improved Noise-Reduction Algorithm

| | |
|---|---|
| Journal: | *Analyst* |
| Manuscript ID: | AN-ART-01-2014-000215.R1 |
| Article Type: | Paper |
| Date Submitted by the Author: | 10-Mar-2014 |
| Complete List of Authors: | Kirimli, Ceyhun; Drexel University, School of Biomedical Engineering, Science, and Health Systems<br>Shih, Wei-Heng; Drexel University, Department of Materials Science and Engineering<br>Shih, Wan; Drexel University, School of Biomedical Engineering, Science, and Health Systems |
| | |

# DNA Hybridization Detection with 100 zM Sensitivity Using Piezoelectric Plate Sensors with Improved Noise-Reduction Algorithm[†]

**Ceyhun E. Kirimli,[a‡] Wei-Heng Shih,[b] and Wan Y. Shih[*c]**

We have examined real-time, in situ hybridization detection of target DNA (tDNA) in a buffer solution and in urine using 8 $\mu$m-thick lead magnesium niobate-lead titanate (PMNPT) piezoelectric plate sensors (PEPSs) about 1.1-1.2 mm long and 0.45 mm wide with improved 3-mercaptopropyltrimethoxysilane (MPS) insulation and a new multiple-parabola ($>$50) resonance peak position fitting algorithm. With probe DNA (pDNA) immobilized on the PEPS surface and by monitoring the first width extension mode (WEM) resonance frequency shift we detected tDNA in real time at concentration as low as $1 \times 10^{-19}M$ in urine ($100zM$) with a signal to noise ratio (SNR) of 13 without DNA isolation and amplification at room temperature in 30 min. The present multiple-parabola fitting algorithm increased the detection SNR by about 10 times from those obtained using the raw data and by about 5 times from those obtained using single parabola fitting. The detection was validated by *in situ* follow-up detection and subsequent visualization of fluorescent reporter microspheres (FRMs) coated with reporter DNA complementary to the tDNA but different from the probe pDNA.

## 1  Introduction

Cell-free DNA was first discovered by Mandel and Metais[1] in 1948 and became increasingly more important when mutant Ras gene fragments were discovered in the blood of patients.[2,3] Since then, circulating DNA in the blood has been studied extensively for its diagnostic and prognostic association with various cancers such as; bladder cancer,[4,5] breast cancer,[6–9] cervical cancer,[10,11] colorectal cancer,[12–16] hepatocellular carcinoma,[17–20] lung cancer,[21–25] lymphoma,[26–28] melanoma,[29–36] ovarian cancer,[37,38] pancreatic cancer,[39,40] and prostate cancer[41–46]. The passage of circulating DNA through the kidney barrier has been overlooked due to the selectivity of the nephron and DNA fragments observed in urine have been mostly thought to have originated from organs and tissues of the urogenital tract. More recently, it has been found that low-molecular weight (LMW) DNA fragments from a distant organ could pass through kidneys[47,48]. The current standard method for detecting DNA is polymerase chain reaction (PCR). For transrenal DNA detection, PCR has limitations on the amplicon size[49] and potential inhibitions by co-isolated factors. Furthermore, the effectiveness of PCR could also be limited by the DNA isolation techniques which are mostly for isolating nuclear DNA from intact cells[48], not particularly suitable for isolating short transrenal DNA fragments[36,48,50]. It would be desirable to have a real-time, label-free method that can detect transrenal DNA fragments in urine that does not depend on the DNA isolation techniques and is not limited by the lengths of the DNA fragments.

Current genetic detection technologies under development rely on fluorescence[51–53], quartz crystal microbalance (QCM)[54,55], electrochemical[56] binding of nano-metal particles[57], surface plasmon resonance (SPR)[58], silicon-based microcantilever sensor as well as piezoelectric microcantilever sensor. For DNA detection, nanoparticle amplified QCM exhibited a concentration sensitivity of $1pM$[59]. Nanoparticle enhanced SPR exhibits concentration sensitivity of $10 - 100$ $aM$[60]. The electrochemical methods involving nanofibers and nanotubes also exhibited concentration sensitivity of about 30 fM[61]. Nanowires[62–66] and nanotubes[67,68] exhibited concentration sensitivity ranging from $100fM$ to $1fM$. Microcantilevers coupled with nano-metal particles exhibited $0.01nM$ concentration sensitivity[69]. Although methods such as QCM, SPR, silicon-based microcantilever sensor as well as lead zirconate titanate (PZT) piezoelectric microcantilver sensor

† Electronic Supplementary Information (ESI) available: [details of any supplementary information available should be included here]. See DOI: 10.1039/b000000x/
*a Lakehead University, Department of Chemistry, Thunder Bay, CANADA, Phone: 1-807-343-8450; E-mail: ckirimli@lakeheadu.ca*
*b Drexel University, Department of Materials Science and Engineering, Philadelphia,Pennsylvania, USA, Phone: 1-215-895-6636, Email: shihwh@drexel.edu*
*c Drexel University, School of Biomedical Engineering, Science, and Health Systems, Philadelphia, Pennsylvania, USA, Phone: 1-215-895-2325, Email: shihwy@drexel.edu*
‡ This work was carried out while a PhD student in the School of Biomedical Engineering, Science, and Health Systems at Drexel University in Philadelphia, PA 19104.
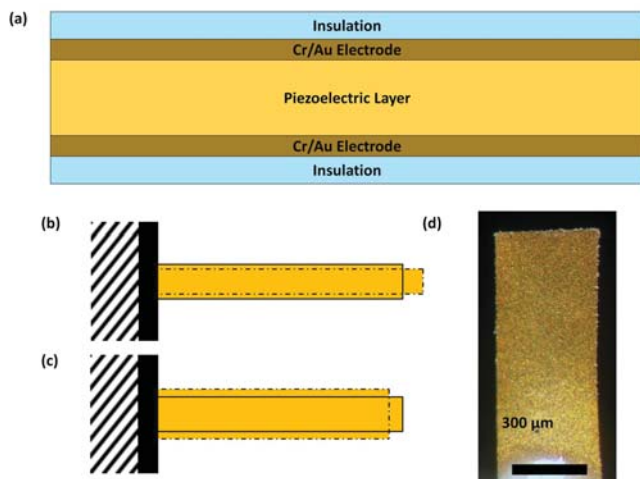∗ Wan Y. Shih is the corresponding author.

**Fig. 1** A schematic of (a) the cross section of a piezoelectric plate sensor (PEPS), (b) the first length extension mode (LEM), (c) width extension mode (WEM) vibration of a PEPS where the solid bars illustrated the initial position of the PEPS and the dashdotted shapes illustrate the extended positions, and (d) a top-view optical micrograph.

(PEMS)[70,71] were label-free, the sensitivity was still many orders of magnitude away from the attomolar ($10^{-18}M$) requirement.[72] Similarly, the $10^{-16}M$ sensitivity achieved by magnetic beads isolation coupled with electrochemical enhancement was not sufficient[73]. Nano-scale mechanical imaging by atomic force microscopy (AFM) can differentiate unhybridized single-stranded DNAs (ssDNAs) from hybridized double-stranded DNAs (dsDNAs) at attomolar sensitivity but it required sophisticated instrument such as AFM[74]. Although a GaN nanowire extended-gate field-effect-transistor could detect attomolar concentrations of target DNA (tDNA) in situ[53] the detection signal (0.2$V$) at $10^{-18}M$ was not very different from that (0.3$V$) at $10^{-6}M$ making it not suitable for DNA quantification. Streptavidin horseradish peroxidase functionalized carbon nanotubes could detect DNA at $10^{-18}M$ however it required labeling and was not in situ[75] while label-free carbon nanotube impedance biosensors could only detect DNA at 100 $aM$, not sufficient for clinical applications[76]. Electrochemical biosensors have been shown to reach attomolar sensitivity. However, they required electrocatalysis[77] or magnetic beads amplification[78] and were thus not label-free or real-time.

Lead magnesium niobate-lead titanate $(Pb(Mg_{1/3}Nb_{2/3})O_3)_{0.65} - (PbTiO_3)_{0.35}$ (PMN-PT) piezoelectric plate sensor (PEPS) is a new type of piezoelectric sensor consisting of solely a PMN-PT freestanding film 8$\mu m$ in thickness[79] thinly coated with a gold electrode on the two major surfaces and encapsulated with a thin *3-mercaptopropyltrimethoxysilane* (MPS) electrical insu-

lation layer Figure 1a. Receptor specific to a biomarker is immobilized on the surface of the electrical insulation layer. Binding of the target biomarker to the receptor on the PEPS surface shifts the PEPS length-extension-mode (LEM) (Figure 1b) or width-extension mode (WEM) (Figure 1c) resonance peak frequency, f. Detection of a target protein or target DNA (tDNA) marker is achieved by directly immersing a PEPS in the biological fluid and monitoring the LEM or WEM resonance frequency shift, $\Delta f$ in real time. What is unique about PMN-PT PEPS is that the detection f is a result of binding stress induced polarization switching within the PMN-PT layer[80], which was typically three orders of magnitude higher than could be accounted for by the mass change alone[81]. As a result, PMN-PT PEPS has shown unprecedented concentration sensitivity of 1.6 $aM$ (960 $copies/ml$) in in situ tDNA detection without the need of amplification[80]. The reason we had different LEM and WEM modes was that we made PEPS longer than it was wide for ease of handling and ease of making. Ideally, one would explore WEM for detection because the higher frequency of WEM could offer better sensitivity. Although , in theory, one could use either the LEM or WEM peak for detection, in past practice, only the LEM peak was usable in liquid. The reason was that the width of the WEM peak was closely related to the transverse electromechanical coupling constant, $-k_{31}$.[81] The better the piezoelectric performance of the PMN-PT layer the wider the WEM peak. For a $-k_{31}$ of about 0.32 the Q value-the ratio of the peak frequency to the width at half the peak height-would be about 10.[81] Such a wide WEM peak at around 3.5$MHz$ coupled with imperfect electrical insulation and insufficient signal processing made tracking any meaningful peak position shift difficult. Recently, Soylu et al. has found that coating the MPS at $pH = 9$ and with trace amount of water reduced the conductivity of the insulation layer by three orders of magnitude[82]. With such improvement, it may be possible to track WEM peak position change with improved peak position fitting algorithm. The advantage of using a WEM peak for detection is that the resonance frequency of a WEM peak is many times higher than that of the LEM peak. As a result, one may be able to further lower the detection concentration limit.

The goal of this study is to investigate how one can use a WEM peak of a PMN-PT PEPS with improved electrical insulation to detect short DNA fragments spiked in urine using a multiple-parabola peak position fitting approach. The hypothesis was that by fitting the WEM peak to more than one parabola with varying number of data points and by averaging the fitted peak positions one would be able to reduce the noise level for more meaningful tracking of the WEM peak frequency shift due to target DNA binding. We will use 1762$T$/1764$A$ Hepatitis B virus double mutation (HBV-DM) as the model tDNA as it was used in the previous study by
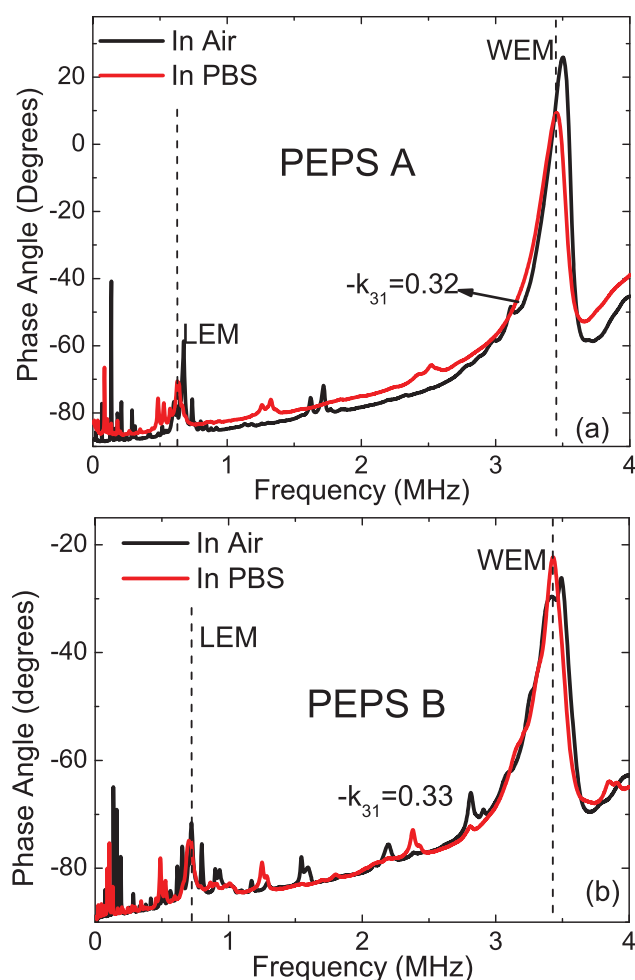
**Fig. 2** In-air (black) and in-PBS (red) phase angle-versus-frequency resonance spectra of PEPS A (a) and PEPS B(b).

an LEM peak with 1.6$aM$ sensitivity.[80] HBV-DM is a hepatitis B viral DNA variant comprised of adenine-1762 to thymine transversion and guanine-1764 to adenine transition which has been previously shown to be a risk factor for the development of Hepatocellular Carcinoma (HCC)[83,84]. A high percentage ($> 60\%$) of HCC patients had HBV-DM in their sera[85,86]. We will show that by fitting the WEM peak to an average of 50 parabolas we could increase the signal (S) to noise (N) ratio, SNR, by more than 10 times over the raw data and more than 5 times over single-parabola fitting and allowed meaningful tracking of the WEM peak frequency shift in real time *in situ* detection of HBV-DM in urine with 100 $zM$(60 *copies*/*ml*) sensitivity without the need of DNA isolation or amplification.

## 2  Experimental

### 2.1  PEPS fabrication

Two PEPS (PEPS A and PEPS B) were used in this study. PEPS A was 1.2$mm$ long and 0.45$mm$ wide and PEPS B was 1.1 $mm$ long and 0.45 $mm$ wide. The geometry of the sensor, about 1 mm long and 0.5 mm wide, was a compromise between ease of fabrication and sensitivity. Presently, the PEPS were fabricated manually. While making the PEPS smaller can increase the LEM and WEM frequencies and potentially further enhance the detection sensitivity it would be hard to accomplish manually. However, it should be noted that with presently available tools and automation, in the future, it is possible to make smaller PEPS. Briefly, PEPS A and PEPS B were fabricated from PMN-PT freestanding films 8 $\mu m$ thick that was coated with 110 $nm$ thick Cr/Au electrodes by thermal evaporation (Thermionics VE 90) and cut into 2.5 $mm$ by 0.45 $mm$ strips by a wire saw (Princeton Scientific Precision, Princeton, NJ). Gold wires 10 $\mu m$ in diameter were glued to the top and bottom electrodes of each strip using conductive glue ($XCE3104XL$, Emerson and Cuming Company, Billerica, MA). The rear end of the strip was fixed on a glass substrate by a nonconductive glue (Loctite 1$C$ Hysol Epoxy Adhesive) to form the PEPS geometry. It was then poled at 15 $KV/cm$ at 90$^o$$C$ for 60 $min$ in an incubator (Digital Control Steel Door Incubator 10 − 180$E$, Quincy Lab). The dielectric constant of the PEPS was measured using an electrical impedance analyzer (Agilent 4294$A$) to be about 1800 with a loss factor of 2.5% − 3.7% at 1$kHz$.

### 2.2  Electrical Insulation

A PEPS was electrically insulated to stabilize the resonance peaks for in-liquid detection by a new 3-mercaptopropyltrimethoxysilane (MPS) (Sigma-Aldrich Co. LLC.) solution coating scheme involving improved MPS cross-linking at pH=9.0 and with water.[82] First, the PEPS was cleaned in a Piranha solution (two parts of 98% sulfuric acid (Fisher) with one part of 30% hydrogen peroxide (Fisher)) for 1 min, followed by rinsing in water and ethanol. Before coating the PEPS with MPS at pH=9.0, we dipped the PEPS in 50 ml of a 0.01-mM MPS solution in ethanol (Fisher) with 0.5% of de-ionized (DI) water for 30 min to promote hydrolysis followed by rinsing with water and ethanol. It was then subject to 5 12-hr of MPS coating in 50$ml$ of a 0.1% MPS solution with 0.5% of DI water in ethanol at pH = 9.0 (adjusted by adding KOH (Fisher)). For each 12-hr of MPS coating, the PEPS was always rinsed with water and ethanol first before being immersed in a fresh 0.1% MPS solution at pH = 9.0 with 0.5% water. At the end of the 5th round of MPS coating, the PEPS was rinsed with DI water and ethanol before further coating with receptors for detection. After
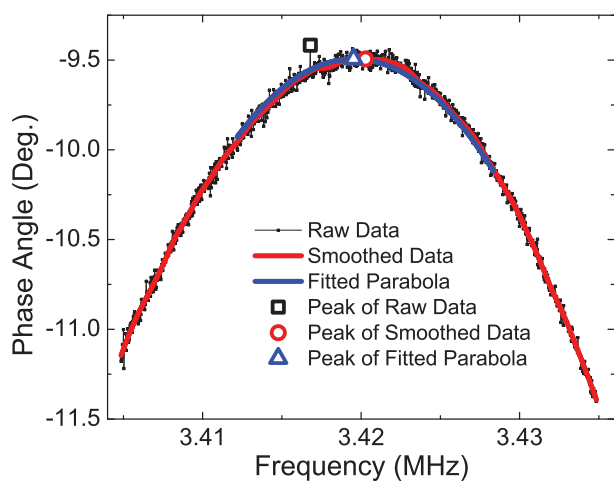
**Fig. 3** Phase angle versus frequency resonance spectra where the raw data and the smoothed data are represented by the black full squares and the red curve, respectively, a parabola fitted using 540 data points is shown as the blue curve. The peak position of the raw data, that of the smoothed data and that of the fitted parabola are shown as the large black full square, red full circle and blue triangle respectively.

insulation, the resonance spectra of the PEPS were measured using a portable AIM 4170C impedance analyzer (Array Solutions).

### 2.3 Resonance peak frequency determination

The phase-angle-versus-frequency resonance spectra of PEPS A and PEPS B in air (black) and in phosphate buffer saline (PBS) solution (red) are shown in Figure 2a and b. Note that PEPS A had a $-k_{31} = 0.32$ and PEPS B had a $-k_{31} = 0.33$ and the WEM peak of PEPS A and PEPS B were both at around 3.5 $MHz$ with a Q of around 10, reminiscent of the high $-k_{31}$ of both PEPSs. Also note that the baselines of the in-air and in-PBS spectra of the PEPSs were less than $1^o - 2^o$ apart, indicative of the effectiveness of the new insulation scheme.

For detection, phase angle-versus-frequency resonance spectra of a PEPS were measured continuously using the AIM 4170C electrical impedance analyzer controlled by a laptop with a custom program written in MatLab. After each resonance-spectrum scan, the MatLab program recorded, analyzed the obtained spectrum, and determined the peak frequency as described below. A resonance peak frequency shift, $\Delta f$, versus time plot on the computer screen was refreshed after each resonance spectrum scan in real time. The program also used the obtained peak frequency shift to adjust the start and stop frequencies for the next resonance-spectrum scan such that the next expected resonance frequency was roughly at the center of frequency window. To determine the peak

**Table 1** The sequences of the tDNA, pDNA, upstream urDNA and downstream drDNA and the melting temperature, $T_m$, of the tDNA with pDNA, that of the tDNA with urDNA, and that of the the tDNA with drDNA

| Type of DNA | Sequence (5′ to 3′) | $T_m$ (C$^o$) |
|---|---|---|
| tDNA$^a$ | 5′…GGTTAA$\underline{T}$$\underline{G}$$\underline{A}$TCTTTGT…3′ | - |
| pDNA | Biotin-5′-ACAAAGAT CATTAACC-3′ | 47 |
| Upstream rDNA (urDNA) | Amine-5′ACAGACCAATTTATG CCTACAGCCTCCTAG-3′ | 76.3 |
| Downstream rDNA (drDNA) | Amine-5′-AATCTCCTCCCCCAA CTCCTCCCAGTCTTT-3′ | 77.4 |

$^a$Mutation sites are indicated by underlined bases

frequency, the raw resonance spectrum (black full squares in Figure 3) was first smoothed by weighted-linear-least-square local regression as illustrated by the red curve in Figure 3. The smoothed curve was then fitted to multiple (about 50) parabolas each with a different frequency range centered at the apparent peak frequency of the smoothed curve. As an example, one of the fitted parabolas is shown as the blue curve in Figure 3 with its peak position denoted by the blue triangle. Each parabola generated a fitted peak frequency. The final fitted peak frequency was the average of all the fitted parabola peak frequencies with outliers [87] excluded.

### 2.4 Target DNA, probe DNA, and reporter DNAs

The tDNA used was the same 200-nucleotide (nt) long single-stranded DNA (Integrated DNA Technologies) used in the previous study [80] containing the nucleotide sequence of the Hepatitis B virus genome (GeneBank Accession #$X$04615) centered around the 1762$T$/1764$A$ double mutations. Part of the sequence of the tDNA that contained the double mutations is shown in Table I where the two mutation sites were underlined. The probe DNA (pDNA) was a *16-nt* long synthetic single-stranded DNA (Sigma) complementary to the *16-nt* sequence of the tDNA centered on the double mutation sites as shown in Table 1. The pDNA had a biotin with a *12-polyethyleneglycol* (PEG) spacer at the 5′ end. The melting temperature of the pDNA to the tDNA was 47$^o$$C$ as estimated under the experimental conditions [88] and listed in Table1.

To immobilize the biotin-activated pDNA on the PEPS surface, the MPS-coated PEPS was first immersed in 200 $\mu l$ of 5 $mg/ml$ of maleimide activated biotin (Maleimide-PEG11-Biotin) (Pierce) in PBS for 30 minutes. The maleimide reacted with the thiol group on the MPS surface to immobilize the biotin on the PEPS surface. It was then followed by immersing the PEPS in 200 $\mu l$ of 1 $\mu M$ of streptavidin in PBS to bind streptavidin to the biotin on the PEPS surface. Afterwards, the PEPS was immersed in 200 $\mu l$ of a 10 $\mu M$ solution
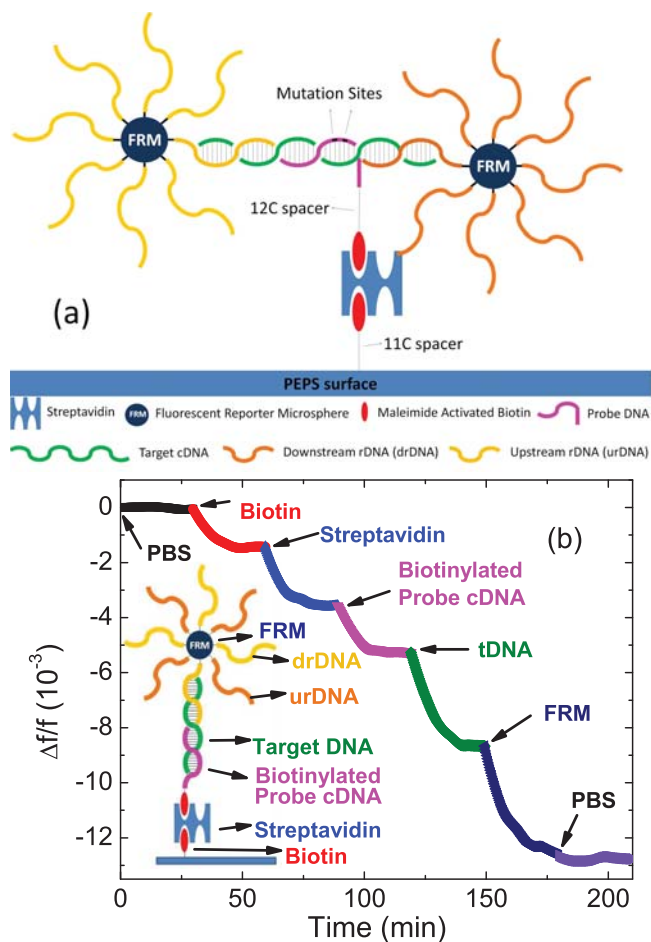
**Fig. 4** (a) A schematic of the relations between tDNA, pDNA, urDNA and drDNA. pDNA is immobilized on PEPS surface using Biotin-Streptavidin-Biotin sandwich. The 200 nts long tDNA (green) hybridizes on pDNA (pink) in the middle and the upstream and downstream flanking regions hybridize with upstream (yellow) and downstream (orange) rDNA which are conjugated on FRMs (dark blue spheres) and (b) relative resonance frequency shift, $\Delta f/f$, of PEPS A during various steps of pDNA immobilization and tDNA detection. The insert in (b) shows a schematic of the molecules involved in the immobilization and detection steps.

of the probe DNA in PBS for an hour to allow the biotin at the $5'$ end of the pDNA to bind to the streptavidin on the PEPS surface. The details of the chemical reaction of the immobilization steps are contained in the supplemental materials.

There were two 30-nt long reporter DNAs (rDNAs) (Sigma). One was complementary to the sequence upstream of what was complementary to the pDNA and the other was complementary to the sequence downstream of what was complementary to the tDNA. The upstream rDNA was amine-activated with a *12-PEG* spacer at the $5'$ end while the down-

stream rDNA was amine-activated with a *7-PEG* spacer at the $3'$ end. The sequence of the upstream rDNA and that of the downstream rDNA are also shown in Table 1. Figure 4(a) is a schematic that illustrates the relationships between the tDNA, the pDNA, the urDNA, and the drDNA. In real DNA fragments, the mutation sites may be located anywhere in the fragments and in some cases the mutated sites may be too close to the edge for strong enough rDNA binding. Under such conditions, an rDNAs in the opposite stream would permit the binding of the rDNA to captured tDNA on the sensor surface. For this reason, we included both upstream and downstream rDNA in the study even though in the present synthetic tDNA the mutation sites were centrally located. The melting temperature for binding the upstream rDNA (urDNA) to the tDNA was $76.3^oC$ and that of the downstream rDNA (drDNA) to the tDNA was $77.4^oC$, which are also listed in Table 1. Both drDNA and urDNA are immobilized on 6 $\mu m$ size fluorescent report microspheres (FRM) as described previously [80,89] for in situ validation as well as for visualization of the detection [80]. In Figure 4(b), we plot the $\Delta f/f$ versus time of PEPS A during the various steps of pDNA immobilization followed by tDNA detection and the subsequent FRM detection. Steps of immobilization are illustrated in inset in Figure 4(b).

## 2.5 Urine Sample Preparation

Urine samples were collected in a 50 $ml$ centrifuge in a first morning sample collection fashion after emptying the bladder the previous evening. Samples are kept in $4^oC$ refrigerator for detection. Blocking of non-specific binding is accomplished by dissolving 3% BSA in urine equilibrated to room temperature.

## 2.6 Flow setup

All the tDNA detections were carried out in a flow. A schematic of the flow system consisting of a polycarbonate detection chamber 18.5 $mm$ long 3.5 $mm$ wide and 5.5 $mm$ deep (volume = 356 $\mu l$), three reservoirs, and a peristaltic pump (Cole-Parmer $77120 - 62$) interconnected with 0.8 $mm$ wide tubing is shown in Figure 5a. The PEPS was vertically placed in the center of the flow chamber with its major faces parallel to the flow as illustrated by the schematic shown in Figure 5b. In each detection event, only one reservoir was connected to the detection chamber. The total volume of the liquid was 50 $ml$ including the liquid in the reservoir, the detection chamber and the connecting tubing. In what follows, all detections were carried out with a flow rate of 1 $ml/min$ corresponding to an average flow velocity of 1.4 $mm/s$ at the PEPS surface. Furthermore, in this setup, the detection could transition from one detection experiment involving the sample in one reservoir to another detection experiment involving the sample of
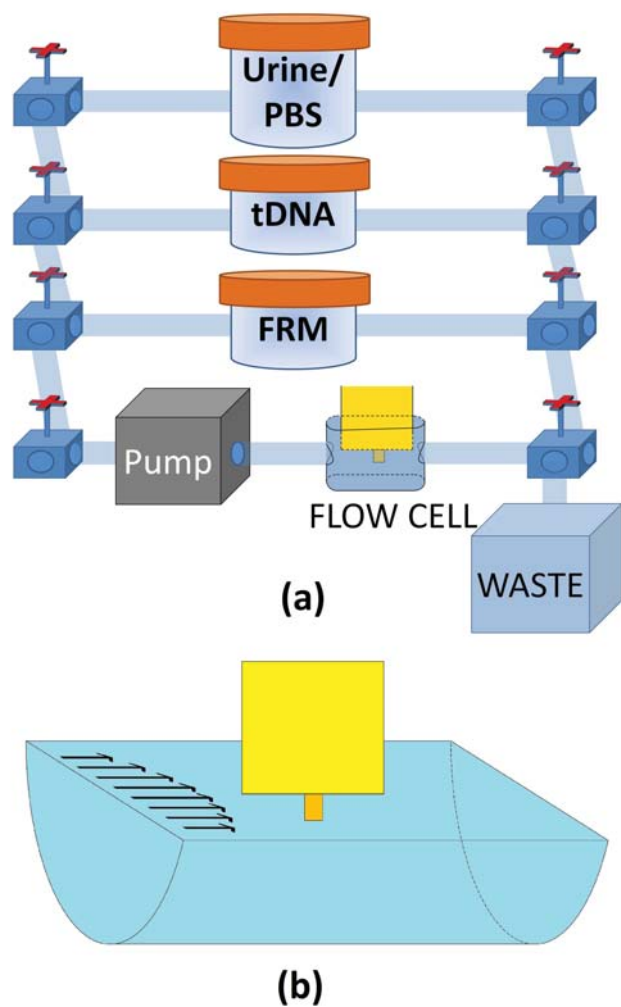
**Fig. 5** (a) A schematic of the flow system and (b) a schematic of the flow cell where the PEPS is placed in the center of the laminar flow.

another reservoir by turning the valves. Typically, a 20-second period for valves turning without data recording was sufficient for a smooth transition from one detection experiment to another.

## 3 Results

The theoretical first WEM and the first LEM resonance peak frequencies could be calculated[80] using $f = c/2w$ and $f = c/4L$, respectively where $c = \sqrt{Y_{11}/\rho}$ was the sound velocity in the piezoelectric layer with $Y_{11} = 81\ GPa$ and $\rho = 7800\ kg/m^3$ being the Youngs modulus in the length and width directions and $\rho$ the density of the piezoelectric layer, respectively and $w$ and $L$ the width and the length of the PEPS, respectively. The theoretical first LEM and WEM peak frequen-
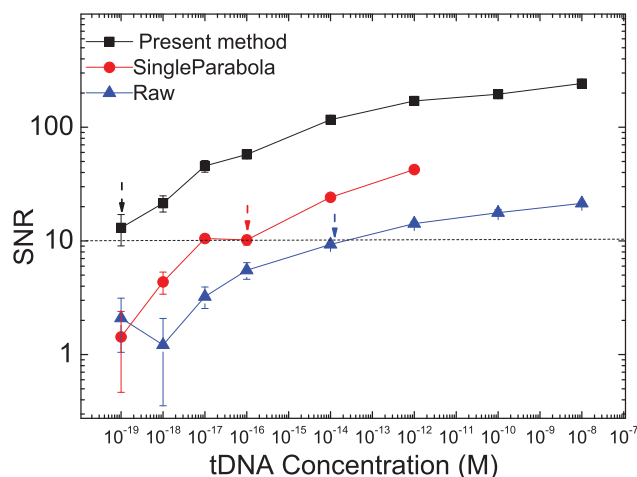


**Fig. 6** Signal to noise ratio (SNR) versus tDNA concentration of tDNA detection in PBS by PEPS A where full squares, full circles, and full triangles denote SNR obtained by the present multiple-parabola fitting algorithm, by single-parabola fitting (red circles), and by raw data, respectively. Arrows indicate the lowest concentrations with an SNR value of 10 for each method

cies were estimated to be $623\ kHz$ and $3.44\ MHz$, respectively for PEPS A and $718\ kHz$ and $3.42\ MHz$, respectively for PEPS B as indicated by the vertical dashed lines in Figures 2(a) and 2(b).

tDNA detection was carried out using PEPS A in PBS with tDNA spiked at various concentrations to compare the signal-to-noise ratio (SNR) of the detection resonance frequency shift obtained by fitting the resonance peak frequency using the present multiple-parabola algorithm to those for the same detection but obtained using the raw data or using a single-parabola algorithm. The tDNA detection was immediately followed by FRM detection at a concentration of $10^5\ FRMs/ml$ as described previously[80]. The tDNA detection $\Delta f/f$ versus time of PEPS A and the corresponding $-\Delta f/f$ at $t = 30$ min versus tDNA concentration are included in the supplemental materials. In the present signal-to-noise (SNR) analysis, the signal was the average tDNA detection $\Delta f/f$ between $t = 25-30$ min and the noise was the standard deviation of $-\Delta f/f$ of the blank sample (i.e., without tDNA). The resultant SNR versus tDNA concentration is shown in Figure 6. Note all data points in Figure 6 were the average of three independent runs for each concentration. As can be seen, the SNR obtained by the present multiple-parabola fitting (full squares) were larger than 10 down to the tDNA concentration of $10^{-19} M$. By convention, the lowest acceptable SNR is 3. The fact that the present detection with the multiple-parabola fitting algorithm exhibited an SNR of 10 at $10^{-19} M$, indicating the high sensitivity of the PEPS detection. For comparison, we
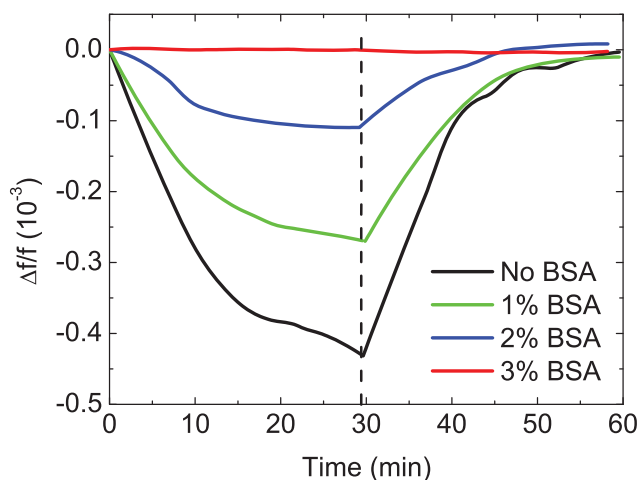
**Fig. 7** Relative frequency shift, $\Delta f/f$, of PEPS B in urine at 1 $ml/min$ for 30 min followed with PBS washing at a flow rate of 6 $ml/min$ after the PEPS was initially blocked with 0, 1, 2 and 3 percent BSA.

also plot the SNR obtained with the raw data (full triangles) and by single-parabola fitting (full circles). As can be seen, the present multiple-parabola fitting algorithm improved the SNR by about ten times from those obtained by the raw data and by about 5 times from those obtained by single-parabola fitting. Note the drop in SNR obtained from the raw data at $10^{-18}M$ was not meaningful, as the SNR at concentrations below $10^{-17}M$ were already below 3 -an indication that SNR values at below $10^{-17}M$ were not reliable. The positive tDNA detection with an SNR of 10 even at a tDNA concentration as low as 60 $copies/ml$ was validated by the FRM detection immediately following the t DNA detection as described in the supplemental materials.

In the following, we applied the multiple-parabola fitting algorithm in the detection of DNA hybridization in urine using PEPS B. To determine the appropriate amount of BSA needed to block the PEPS surface from nonspecific binding, PEPS was first treated with a BSA solution of concentration ranging $0 - 3\%$ followed by inserting the PEPS in flowing urine at a 1 $ml/min$ flow rate for 30 $min$ followed by flowing a phosphate buffer saline (PBS) solution at a 6 $ml/min$ flow rate for 30 $min$. The resultant $\Delta f/f$ versus time in urine and the subsequent PBS washing with various amounts of BSA blocking is shown in Figure 7. As can be seen, without BSA blocking, $\Delta f/f$ decreased in urine and was subsequently recovered after PBS washing, indicating that the $\Delta f/f$ in urine was due to nonspecific binding by urine which could be washed off by flowing PBS. The nonspecific binding decreased with an increasing concentration of BSA blocking and with 3% BSA blocking it appeared that nonspecific binding by the urine no
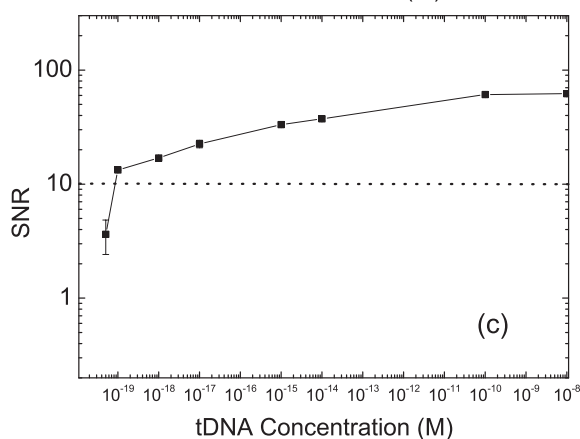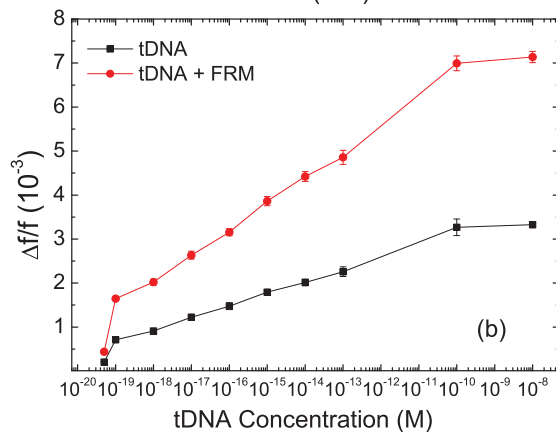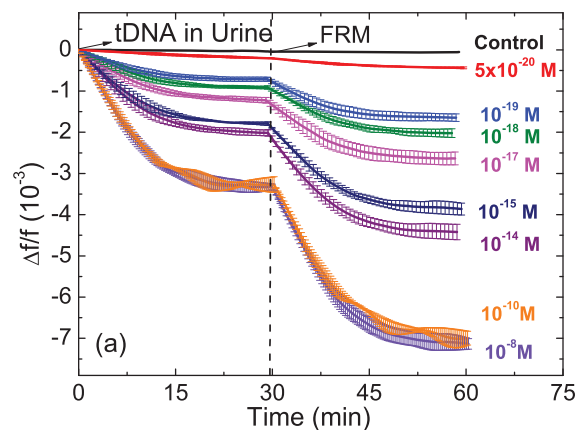


**Fig. 8** (a) Relative resonance frequency shift, $\Delta f/f$ versus time of tDNA detection at various concentrations in urine and (b) $-\Delta f/f$ at $t = 30min$ (tDNA hybridization) and at $t = 60min$ (tDNA hybridization plus FRM detection) versus tDNA concentration. (c) SNR versus concentration of tDNA graph plotted using data in part (a)

longer occurred, i. e, there was no resonance frequency down shifting in urine and no resonance frequency up shifting in PBS. In what follows, all detection will be carried out with
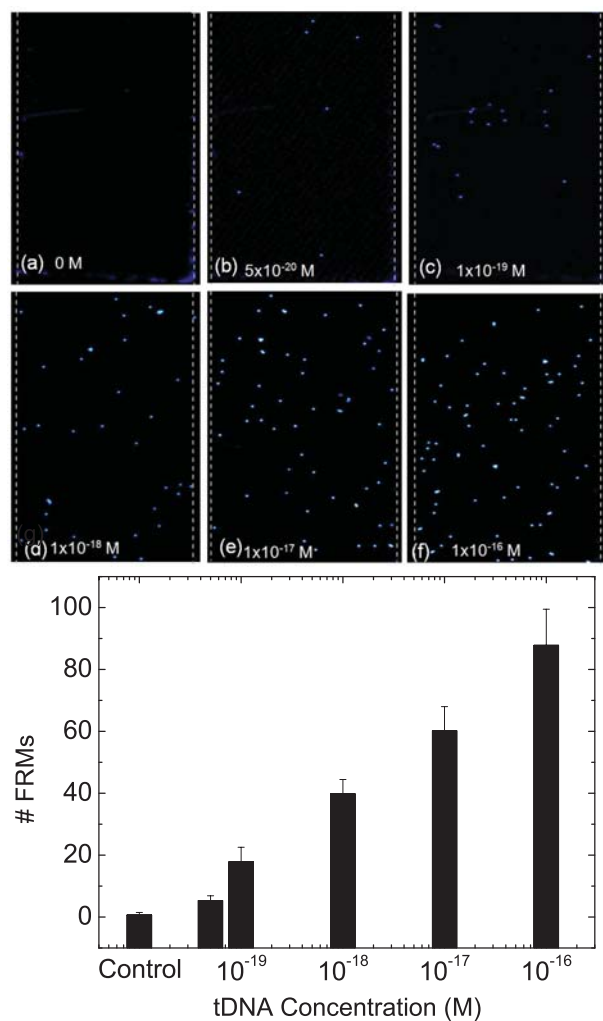
3% BSA blocking.



**Fig. 9** Fluorescent micrographs of the PEPS surface after FRM detection followed by (a) ) $0\,M$, (b) $5\times10^{-20}M$, (c) $1\times10^{-19}M$, (d) $1\times10^{-18}M$, (e) $1\times10^{-17}M$ and (f) $1\times10^{-16}M$ of tDNA detection. The width of PEPS B as denoted by the parallel dashed lines was $450\,\mu m$. Clearly the number of FRMs captured on the PEPS surface increased with an increasing tDNA concentration in a dose responsive fashion validating the tDNA detection at a concentration as low as $5\times10^{-20}M$. (g) Average number of FRMs captured on the PEPS surface versus tDNA concentration in urine.

Figure 8a shows the $\Delta f/f$ versus time of the tDNA detection in urine at $t=0-30$ min followed by FRM detection at $t=30-60$ min for tDNA concentrations of $0,5\times10^{-20},10^{-19},10^{-18},10^{-17},10^{-15},10^{-14},10^{-10}$, and $10^{-8}M\,(0,30,60,600,6,000,6\times10^5,6\times10^6,6\times10^{10}$ and $6\times10^{12}\,copies/ml)$. Note that all the data points shown in Figure 8a were the average of three independent detections at each tDNA concentration. As can be seen, $\Delta f/f$ decreased

with time in a dose responsive fashion. In addition, $\Delta f/f$ further decreased during the subsequent FRM detection validating that the $\Delta f/f$ observed during the tDNA detection was indeed due to the binding of the tDNA to the pDNA on the PEPS surface. The $-\Delta f/f$ at $t=30$ min after tDNA detection and the $-\Delta f/f$ after FRM detection at $t=60$ min are plotted versus tDNA concentration in Figure 8b. Clearly, the $-\Delta f/f$ of tDNA detection ranges from $0.19\times10^{-3}$ at $5\times10^{-20}M$ (30 $copies/ml$) to $>3.3\times10^{-3}$ when saturated at $10^{-10}$ and $10^{-8}$ M. Figures 8a and 8b clearly illustrate that PEPS exhibited a 10-decade dynamic range in DNA detection in urine. Furthermore, from Figure 8b, one can see that the $-\Delta f/f$ of the FRM detection following the tDNA was directly proportional to that of tDNA detection alone, validating that the tDNA detection was indeed due to the binding of the tDNA to the pDNA on the PEPS surface. The SNR of the tDNA detection by PEPS B in urine was similarly analyzed where the signal denotes the average tDNA detection $\Delta f/f$ between $t=25-30$ min and noise the standard deviation of $-\Delta f/f$ of the blank sample (i.e., without tDNA). The resultant SNR versus tDNA concentration is shown in Figure 8c. The SNR of the lowest concentration, $5\times10^{-20}M$, was slightly above 3 with a standard deviation. For this reason the limit of detection for this study was chosen as $1\times10^{-19}M$ or approximately 60 $copies/ml$. Further visual validation was carried out by examining the PEPS surface under a fluorescent microscope (Olympus BX51). Fluorescent micrographs of the FRMs captured on the PEPS surface following tDNA detection at various tDNA concentrations are shown in Figure 9. As can be seen, the number of FRMs captured on the PEPS surface increased with an increasing tDNA concentration in a dose responsive fashion, further validating PEPS tDNA detection. The average number of FRMs on the PEPS surface versus tDNA concentration is also shown in Figure 9g where each data point was the average of 6 images obtained at the same tDNA concentration

## 4  Discussions

That a 60 $copies/ml$ analytical sensitivity was achieved by both PEPS A in PBS and PEPS B in urine may be attributed to the similar $-k_{31}$ between PEPS A (0.32) and PEPS B (0.33). The sensitivity of a PEPS was related to its $-k_{31}$: The higher the $-k_{31}$ the more sensitive the PEPS.[81] With results from both PEPS B and PEPS A it suffices to say that with improved MPS insulation and using the present multiple-parabola fitting algorithm a PEPS with $-k_{31}\geq0.32$ exhibit an analytical sensitivity of better than 60 $copies/ml$, which was $\geq16$ times lower than that of the previous same tDNA detection in PBS using a PEPS of a similar $-k_{31}$ but with only single-parabola fitting.

## 5 Conclusions

We have examined real-time, *in* situ hybridization detection of tDNA in a buffer solution and in urine using 8 $\mu m$-thick PMN-PT PEPSs about $1.1 - 1.2$ $mm$ long and $0.45$ $mm$ wide with improved MPS insulation and a new multiple-parabola ($> 50$) resonance peak position fitting algorithm. With pDNA immobilized on the PEPS surface and by monitoring the first width extension mode (WEM) resonance frequency shift we detected tDNA in real time at concentration as low as $1 \times 10^{-19} M$ in urine (100 $zM$) with an SNR of $> 10$ without DNA isolation and amplification at room temperature in 30 min. Note there was no incubation time. 30 min was between the time when the sample was loaded and the time when we stopped the monitoring. The present multiple-parabola fitting algorithm increased the detection SNR by about 10 times from those obtained using the raw data and by about 5 times from those obtained using single parabola fitting. The detection was validated by *in situ* follow-up detection and subsequent visualization of FRMs coated with reporter DNA complementary to the tDNA but different from the pDNA.

## 6 Acknowledgment

## References

1 P. Mandel, *CR Acad Sci Paris*, 1948, **142**, 241–243.

2 G. D. Sorenson, D. M. Pribish, F. H. Valone, V. A. Memoli, D. J. Bzik and S. L. Yao, *Cancer Epidemiology Biomarkers and Prevention*, 1994, **3**, 67–71.

3 V. Vasioukhin, P. Anker, P. Maurice, J. Lyautey, C. Lederrey and M. Stroun, *Br J Haematol*, 1994, **86**, 774–9.

4 M. T. Valenzuela, R. Galisteo, A. Zuluaga, M. Villalobos, M. I. Nunez, F. J. Oliver and J. M. Ruiz de Almodovar, *Eur Urol*, 2002, **42**, 622–8; discussion 628–30.

5 M. Utting, W. Werner, R. Dahse, J. Schubert and K. Junker, *Clin Cancer Res*, 2002, **8**, 35–40.

6 H. Schwarzenbach, K. Pantel, B. Kemper, C. Beeger, F. Otterbach, R. Kimmig and S. Kasimir-Bauer, *Breast Cancer Res*, 2009, **11**, R71.

7 J. M. Silva, J. Silva, A. Sanchez, J. M. Garcia, G. Dominguez, M. Provencio, L. Sanfrutos, E. Jareo, A. Colas, P. Espaa and F. Bonilla, *Clinical Cancer Research*, 2002, **8**, 3761–3766.

8 B. Taback, A. E. Giuliano, N. M. Hansen, F. R. Singer, S. Shu and D. S. Hoon, *Cancer Res*, 2003, **63**, 1884–7.

9 N. Umetani, A. E. Giuliano, S. H. Hiramatsu, F. Amersi, T. Nakagawa, S. Martino and D. S. Hoon, *J Clin Oncol*, 2006, **24**, 4270–6.

10 A. Widschwendter, H. M. Muller, H. Fiegl, L. Ivarsson, A. Wiedemair, E. Muller-Holzner, G. Goebel, C. Marth and M. Widschwendter, *Clin Cancer Res*, 2004, **10**, 565–71.

11 W. Pornthanakasem, K. Shotelersuk, W. Termrungruanglert, N. Voravud, S. Niruthisard and A. Mutirangura, *BMC Cancer*, 2001, **1**, 2.

12 T. Lecomte, A. Berger, F. Zinzindohou, S. Micard, B. Landi, H. Blons, P. Beaune, P.-H. Cugnenc and P. Laurent-Puig, *International Journal of Cancer*, 2002, **100**, 542–548.

13 B. Lefebure, F. Charbonnier, F. Di Fiore, J. J. Tuech, F. Le Pessot, F. Michot, P. Michel and T. Frebourg, *Ann Surg*, 2010, **251**, 275–80.

14 B. M. Ryan, F. Lefort, R. McManus, J. Daly, P. W. Keeling, D. G. Weir and D. Kelleher, *Gut*, 2003, **52**, 101–8.

15 N. Umetani, J. Kim, S. Hiramatsu, H. A. Reber, O. J. Hines, A. J. Bilchik and D. S. Hoon, *Clin Chem*, 2006, **52**, 1062–9.

16 T. deVos, R. Tetzner, F. Model, G. Weiss, M. Schuster, J. Distler, K. V. Steiger, R. Grtzmann, C. Pilarsky, J. K. Habermann, P. R. Fleshner, B. M. Oubre, R. Day, A. Z. Sledziewski and C. Lofton-Day, *Clin Chem*, 2009, **55**, 1337–1346.

17 K. Szymanska, O. A. Lesi, G. D. Kirk, O. Sam, P. Taniere, J. Y. Scoazec, M. Mendy, M. D. Friesen, H. Whittle, R. Montesano and P. Hainaut, *Int J Cancer*, 2004, **110**, 374–9.

18 G. D. Kirk, O. A. Lesi, M. Mendy, K. Szymanska, H. Whittle, J. J. Goedert, P. Hainaut and R. Montesano, *Oncogene*, 2005, **24**, 5858–67.

19 K. C. A. Chan, P. B. S. Lai, T. S. K. Mok, H. L. Y. Chan, C. Ding, S. W. Yeung and Y. M. D. Lo, *Clin Chem*, 2008, **54**, 1528–1536.

20 I. H. Wong, Y. M. Lo, W. Yeo, W. Y. Lau and P. J. Johnson, *Clin Cancer Res*, 2000, **6**, 3516–21.

21 S. Wang, T. An, J. Wang, J. Zhao, Z. Wang, M. Zhuo, H. Bai, L. Yang, Y. Zhang, X. Wang, J. Duan, Y. Wang, Q. Guo and M. Wu, *Clin Cancer Res*, 2010, **16**, 1324–30.

22 A. Bearzatto, D. Conte, M. Frattini, N. Zaffaroni, F. Andriani, D. Balestra, L. Tavecchio, M. G. Daidone and G. Sozzi, *Clin Cancer Res*, 2002, **8**, 3782–7.

23 Y. Liu, Q. An, L. Li, D. Zhang, J. Huang, X. Feng, S. Cheng and Y. Gao, *Carcinogenesis*, 2003, **24**, 1897–901.

24 J. L. Ramirez, R. Rosell, M. Taron, M. Sanchez-Ronco, V. Alberola, R. de Las Penas, J. M. Sanchez, T. Moran, C. Camps, B. Massuti, J. J. Sanchez, F. Salazar and S. Catot, *J Clin Oncol*, 2005, **23**, 9105–12.

25 G. Sozzi, D. Conte, L. Mariani, S. Lo Vullo, L. Roz, C. Lombardo, M. A. Pierotti and L. Tavecchio, *Cancer Res*, 2001, **61**, 4675–4678.

26 G. Hosny, N. Farahat and P. Hainaut, *Cancer Lett*, 2009, **275**, 234–9.

27 W. Y. Au, A. Pang, C. Choy, C. S. Chim and Y. L. Kwong, *Blood*, 2004, **104**, 243–9.

28 K. I. Lei, L. Y. Chan, W. Y. Chan, P. J. Johnson and Y. M. Lo, *Clin Cancer Res*, 2002, **8**, 29–34.

29 R. E. Board, G. Ellison, M. C. Orr, K. R. Kemsley, G. McWalter, L. Y. Blockley, S. P. Dearden, C. Morris, M. Ranson, M. V. Cantarini, C. Dive and A. Hughes, *Br J Cancer*, 2009, **101**, 1724–30.

30 A. Fujimoto, S. J. O'Day, B. Taback, D. Elashoff and D. S. Hoon, *Cancer Res*, 2004, **64**, 4085–8.

31 Y. Fujiwara, D. D. Chi, H. Wang, P. Keleman, D. L. Morton, R. Turner and D. S. Hoon, *Cancer Res*, 1999, **59**, 1567–71.

32 B. Taback, Y. Fujiwara, H. J. Wang, L. J. Foshag, D. L. Morton and D. S. Hoon, *Cancer Res*, 2001, **61**, 5723–6.

33 B. Taback, S. J. O'Day, P. D. Boasberg, S. Shu, P. Fournier, R. Elashoff, H. J. Wang and D. S. Hoon, *J Natl Cancer Inst*, 2004, **96**, 152–6.

34 M. Shinozaki, S. J. O'Day, M. Kitago, F. Amersi, C. Kuo, J. Kim, H. J. Wang and D. S. Hoon, *Clin Cancer Res*, 2007, **13**, 2068–74.

35 K. Koyanagi, T. Mori, S. J. O'Day, S. R. Martinez, H. J. Wang and D. S. Hoon, *Cancer Res*, 2006, **66**, 6111–7.

36 T. Mori, S. J. O'Day, N. Umetani, S. R. Martinez, M. Kitago, K. Koyanagi, C. Kuo, T. L. Takeshima, R. Milford, H. J. Wang, V. D. Vu, S. L. Nguyen and D. S. Hoon, *J Clin Oncol*, 2005, **23**, 9351–8.

37 H. M. Muller, S. Millinger, H. Fiegl, G. Goebel, L. Ivarsson, A. Widschwendter, E. Muller-Holzner, C. Marth and M. Widschwendter, *Clin Chem*, 2004, **50**, 2171–3.

38 R. Zachariah, S. Schmid, N. Buerki, R. Radpour, W. Holzgreve and X. Zhong, *Obstet Gynecol*, 2008, **112**, 843 – 50.

39  T. Liggett, A. Melnikov, Q. L. Yi, C. Replogle, R. Brand, K. Kaul, M. Talamonti, R. A. Abrams and V. Levenson, *Cancer*, 2010, **116**, 1674–80.

40  A. Castells, P. Puig, J. Mora, J. Boadas, L. Boix, E. Urgell, M. Sole, G. Capella, F. Lluis, L. Fernandez-Cruz, S. Navarro and A. Farre, *J Clin Oncol*, 1999, **17**, 578–84.

41  P. J. Bastian, G. S. Palapattu, X. Lin, S. Yegnasubramanian, L. A. Mangold, B. Trock, M. A. Eisenberger, A. W. Partin and W. G. Nelson, *Clin Cancer Res*, 2005, **11**, 4037–43.

42  M. Roupret, V. Hupertan, J. W. Catto, D. R. Yates, I. Rehman, L. M. Proctor, J. Phillips, M. Meuth, O. Cussenot and F. C. Hamdy, *Int J Cancer*, 2008, **122**, 952–6.

43  J. Ellinger, P. J. Bastian, K. I. Haan, L. C. Heukamp, R. Buettner, R. Fimmers, S. C. Mueller and A. von Ruecker, *International Journal of Cancer*, 2008, **122**, 138–143.

44  H. Schwarzenbach, C. Alix-Panabires, I. Mller, N. Letang, J.-P. Vendrell, X. Rebillard and K. Pantel, *Clinical Cancer Research*, 2009, **15**, 1032–1038.

45  E. Sunami, M. Shinozaki, C. S. Higano, R. Wollman, T. B. Dorff, S. J. Tucker, S. R. Martinez, R. Mizuno, F. R. Singer and D. S. Hoon, *Clin Chem*, 2009, **55**, 559–67.

46  N. Mehra, M. Penning, J. Maas, N. van Daal, R. H. Giles and E. E. Voest, *Clin Cancer Res*, 2007, **13**, 421–6.

47  I. Botezatu, O. Serdyuk, G. Potapova, V. Shelepov, R. Alechina, Y. Molyaka, V. Ananev, I. Bazin, A. Garin, M. Narimanov, V. Knysh, H. Melkonyan, S. Umansky and A. Lichtenstein, *Clin Chem*, 2000, **46**, 1078–84.

48  S. R. Umansky and L. D. Tomei, *Expert Rev Mol Diagn*, 2006, **6**, 153–63.

49  Y. H. Su, M. Wang, T. M. Block, O. Landt, I. Botezatu, O. Serdyuk, A. Lichtenstein, H. Melkonyan, L. D. Tomei and S. Umansky, *Ann N Y Acad Sci*, 2004, **1022**, 81–9.

50  A. Melnikov, D. Scholtens, A. Godwin and V. Levenson, *J Mol Diagn*, 2009, **11**, 60–5.

51  D. M. Hammond, A. Manetto, J. Gierlich, V. A. Azov, P. M. Gramlich, G. A. Burley, M. Maul and T. Carell, *Angew Chem Int Ed Engl*, 2007, **46**, 4184–7.

52  F. Guo, M. I. Lapsley, A. A. Nawaz, Y. Zhao, S.-C. S. Lin, Y. Chen, S. Yang, X.-Z. Zhao and T. J. Huang, *Analytical Chemistry*, 2012, **84**, 10745–10749.

53  Y. Chen and T. S. Seo, *ELECTROPHORESIS*, 2011, **32**, 1456–1464.

54  M. Passamano and M. Pighini, *Sensors and Actuators B: Chemical*, 2006, **118**, 177–181.

55  K. Feng, J. Li, J. H. Jiang, G. L. Shen and R. Q. Yu, *Biosens Bioelectron*, 2007, **22**, 1651–7.

56  R. Gasparac, B. J. Taft, M. A. Lapierre-Devlin, A. D. Lazareck, J. M. Xu and S. O. Kelley, *Journal of the American Chemical Society*, 2004, **126**, 12270–12271.

57  S. J. Park, T. A. Taton and C. A. Mirkin, *Science*, 2002, **295**, 1503–6.

58  L. He, M. D. Musick, S. R. Nicewarner, F. G. Salinas, S. J. Benkovic, M. J. Natan and C. D. Keating, *Journal of the American Chemical Society*, 2000, **122**, 9071–9077.

59  X. Mao, L. Yang, X. L. Su and Y. Li, *Biosens Bioelectron*, 2006, **21**, 1178–85.

60  L. K. Gifford, I. E. Sendroiu, R. M. Corn and A. Luptak, *J Am Chem Soc*, 2010, **132**, 9265–7.

61  T. Yang, N. Zhou, Y. Zhang, W. Zhang, K. Jiao and G. Li, *Biosens Bioelectron*, 2009, **24**, 2165–70.

62  G. Zheng, F. Patolsky, Y. Cui, W. U. Wang and C. M. Lieber, *Nat Biotechnol*, 2005, **23**, 1294–301.

63  G. J. Zhang, Z. H. Luo, M. J. Huang, G. K. Tay and E. J. Lim, *Biosens Bioelectron*, 2010, **25**, 2447–53.

64  A. Andreu, J. W. Merkert, L. A. Lecaros, B. L. Broglin, J. T. Brazell and M. El-Kouedi, *Sensors and Actuators B: Chemical*, 2006, **114**, 1116–1120.

65  Z. Gao, A. Agarwal, A. D. Trigg, N. Singh, C. Fang, C. H. Tung, Y. Fan, K. D. Buddharaju and J. Kong, *Anal Chem*, 2007, **79**, 3291–7.

66  J.-i. Hahm and C. M. Lieber, *Nano Letters*, 2003, **4**, 51–54.

67  J. Wang, R. Polsky, A. Merkoci and K. L. Turner, *Langmuir*, 2003, **19**, 989–991.

68  H. Chang, Y. Yuan, N. Shi and Y. Guan, *Anal Chem*, 2007, **79**, 5111–5.

69  M. Su, S. Li and V. P. Dravid, *Applied Physics Letters*, 2003, **82**, 3562–3564.

70  K. Rijal and R. Mutharasan, *Anal Chem*, 2007, **79**, 7392–7400.

71  S. Zheng, J. H. Choi, S. M. Lee, K. S. Hwang, S. K. Kim and T. S. Kim, *Lab on a Chip*, 2011, **11**, 63–69.

72  F. Caruso, E. Rodda, D. N. Furlong, K. Niikura and Y. Okahata, *Anal Chem*, 1997, **69**, 2043–9.

73  J. Wang, A. N. Kawde and M. Musameh, *Analyst*, 2003, **128**, 912–916.

74  S. Husale, H. H. Persson and O. Sahin, *Nature*, 2009, **462**, 1075–8.

75  W. Gao, H. Dong, J. Lei, H. Ji and H. Ju, *Chem Commun (Camb)*, 2011, **47**, 5220–2.

76  T. Kurkina, A. Vlandas, A. Ahmad, K. Kern and K. Balasubramanian, *Angew Chem Int Ed Engl*, 2011, **50**, 3710–4.

77  L. Soleymani, Z. Fang, S. O. Kelley and E. H. Sargent, *Applied Physics Letters*, 2009, **95**, 143701–3.

78  O. A. Loaiza, S. Campuzano, M. Pedrero, M. I. Pividori, P. Garcia and J. M. Pingarron, *Anal Chem*, 2008, **80**, 8239–45.

79  W. Y. Shih, H. Luo, H. Li, C. Martorano and W.-H. Shih, *Applied Physics Letters*, 2006, **89**, 242913–3.

80  W. Wu, C. E. Kirimli, W. H. Shih and W. Y. Shih, *Biosens Bioelectron*, 2013, **43**, 391–9.

81  W. Wu, W. Y. Shih and W. H. Shih, *Journal of Applied Physics*, 2013, **114**, year.

82  M. C. Soylu, W.-H. Shih and W. Y. Shih, *Industrial and Engineering Chemistry Research*, 2013, **52**, 2590–2597.

83  A. Munoz, J. G. Chen, P. A. Egner, M. L. Marshall, J. L. Johnson, M. F. Schneider, J. H. Lu, Y. R. Zhu, J. B. Wang, T. Y. Chen, T. W. Kensler and J. D. Groopman, *Carcinogenesis*, 2011, **32**, 860–5.

84  J. M. Yuan, A. Ambinder, Y. Fan, Y. T. Gao, M. C. Yu and J. D. Groopman, *Cancer Epidemiol Biomarkers Prev*, 2009, **18**, 590–4.

85  P. Arbuthnot and M. Kew, *International Journal of Experimental Pathology*, 2001, **82**, 77–100.

86  S. Y. Kuang, P. E. Jackson, J. B. Wang, P. X. Lu, A. Munoz, G. S. Qian, T. W. Kensler and J. D. Groopman, *Proc Natl Acad Sci U S A*, 2004, **101**, 3575–80.

87  ASTM Standard E178-08, 2008, Standard Practice for Dealing With Outlying Observations, ASTM International, West Conshohocken, PA, 2008, DOI: 10.1520/E0178-08, www.astm.org.

88  W. A. Kibbe, *Nucleic Acids Res*, 2007, **35**, W43–W46.

89  C. E. Kirimli, W. H. Shih and W. Y. Shih, *Analyst*, 2013, **138**, 6117–26.